ARTICLES

Dimerization of single selenium chains confined in nanochannels of cancrinite: An x-ray absorption study

A. V. Kolobov*
Joint Research Center for Atom Technology–National Institute for Advanced Interdisciplinary Research, 1-1-4, Higashi, Tsukuba, Ibaraki 305, Japan
and Electrotechnical Laboratory, 1-1-4, Umezono, Tsukuba, Ibaraki 305, Japan

H. Oyanagi
Electrotechnical Laboratory, 1-1-4, Umezono, Tsukuba, Ibaraki 305, Japan

V. V. Poborchii*
Joint Research Center for Atom Technology–Angstrom Technology Partnership, 1-1-4, Higashi, Tsukuba, Ibaraki 305, Japan

K. Tanaka
Joint Research Center for Atom Technology–National Institute for Advanced Interdisciplinary Research, 1-1-4, Higashi, Tsukuba, Ibaraki 305, Japan

(Received 30 March 1998; revised manuscript received 4 August 1998)

Local structure of selenium confined in nanochannels of cancrinite (Can-Se) single crystal and powder samples have been studied by polarized x-ray absorption. The spectra for a single crystal are strongly anisotropic implying linear arrangement of Se species. Polarization dependence of extended x-ray absorption fine structure (EXAFS) data provides direct evidence that dimers with the bond length of 2.40 ± 0.01 Å are formed. Polarized x-ray absorption near-edge structure (XANES) spectra demonstrate that they are aligned along the channel of cancrinite. Deconvolution of XANES spectra into Lorentzians (localized states) and the remaining steplike function (continuous states) shows that two localized state peaks are present. While the one polarized parallel to the cancrinite axis is strongly polarized, the other one is essentially isotropic. Comparison of XANES peak positions for Can-Se with that for bulk selenium provides evidence for negative charge on dimers. Despite strong temperature dependence of Raman-scattering spectra found earlier, EXAFS data do not exhibit any noticeable temperature dependence. Possible mechanisms for dimer stabilization are discussed. [S0163-1829(99)09713-1]

I. INTRODUCTION

Interest in low-dimensional nanosize phenomena has been continuously growing in the recent years. One of the promising ways to fabricate such new objects consists in stabilization of individual molecules and nanosize clusters in a matrix of microporous materials.[1–3] Recently, numerous efforts have been put into fabrication of such nanoobjects confined in various zeolite matrices with the characteristic cage size of about 10 Å. Selenium, which in bulk forms consists of chains and/or rings held together by weak Van der Waals interaction, is one of the candidate materials. Confinement of individual chains in zeolite-channel-like pores can provide a new class of quasi-one-dimensional materials. They are expected to have new physical properties that can be controlled through variation of the zeolite framework and/or further doping.

Selenium was shown to be efficiently confined in various zeolites forming either nanosize clusters or one-dimensional isolated chains. Details are given in a recent review.[4] Recently, Se was shown to be confined in cancrinite, which has parallel channels (diameter of ~7 Å) formed by 12-membered rings made of $(Si, Al)O_4$ tetraedra.[4–10] We shall use the notation ''Can-Se'' to refer to this material containing selenium molecules in the channels throughout this paper. Results of previous optical studies[6] indicated that selenium forms *linear* (as opposed to helical) chains in the channels of cancrinite while Raman spectroscopy and x-ray diffraction studies[6–10] suggested the presence of dimers. The structure of Can-Se according to previous studies is shown in Fig. 2 of Ref. 10.

In order to investigate the nature of the Se-chain molecule, we have studied the local structure of Can-Se using polarized extended x-ray absorption fine structure (EXAFS) and x-ray absorption near-edge structure (XANES). Some of the initial results have been reported elsewhere.[1] In this paper, we report full details of the x-ray absorption study, which provides direct evidence for highly oriented Se dimers along the channels of cancrinite. Based on the novel local structure, we discuss the electron states and the mechanism of the dimer formation in the cancrinite channels.

 ©1999 The American Physical Society

II. EXPERIMENTAL DETAILS

The Can-Se samples were similar to those used in earlier studies.[4–11] Se was introduced into the (hydro)cancrinite [the unit cell formula $Na_8Si_6Al_6O_{24}(OH)_2 \cdot 2H_2O$] single crystals (size 1 mm×1 mm×3 mm) from the vapor phase at a temperature of about 500 °C after dehydration at the same temperature. Powdered samples obtained by crushing a small single crystal prior to the measurement were also studied.

A double crystal Si(111) monochromator designed for a high heat-load wiggler at BL13 of the Photon Factory[12] was used. For crystal cooling, an improved version of direct water-cooling mechanism[13] was used.[14] The energy resolution is dependent on the vertical beam divergence and the crystal rocking curve width.

In order to avoid degradation of the energy resolution due to the broadening of the width of a double crystal rocking curve as a result of heat load, the magnetic field of the 27-pole wiggler magnet[15] B_0 was limited to 1.0 T, which amounts to $\frac{2}{3}$ of the full power (5.4 kW) with $B_0 = 1.5$ T. The measured energy resolution at the Cu *K*-edge (8.980 keV) was 2.0 eV with a partially limited vertical beam size. Extrapolating the function to the Se *K*-edge energy, the energy resolution is expected to be approximately 4 eV at 12.658 keV.

The stability of energy position was monitored by the independent XANES measurements of reference materials, i.e., copper foil for 8.9803 keV and *a*-Se thin film for 12.658 keV, the former being the calibration point. It was found that the energy scale was stable during the experiment extending to six days within ±0.0002 degrees in Bragg angle, which amounts to approximately 0.57 eV in uncertainty. For XANES spectra, measurements were sequentially performed during the same fill for which uncertainty in an energy scale was estimated to be less than 0.5 eV.

All measurements for cancrinite samples including powder samples and *a*-Se (1000 Å film) as a reference material on the Se *K*-edge were performed in a fluorescence mode. As a fluorescence x-ray detector, we have used a 19-element pure Ge detector and 9-element NaI(T1) detector arrays. Details of Ge and NaI detectors are given elsewhere.[16,17] The output of single-channel analyzer for each detector channel was recorded in 12-channel CAMAC counters and normalized by the incident beam intensity measured by an ionization chamber filled with dry nitrogen gas.

The sample was mounted on an aluminum holder in an evacuated cryostat equipped with windows for incident and fluorescent x-ray beams. A closed-cycle He refrigerator with a cooling power of ~9 W at 20 K was used.

Se *K*-edge EXAFS and XANES spectra were measured in the temperature range from 20 to 300 K. The angular dependence of the pre-edge and the near-edge features around a strong white line peak at 12 672 eV for the single crystal was sequentially measured at room temperature.

A film of amorphous selenium (*a*-Se) was used as a standard to obtain experimental phase-shift function for the Se-Se pair and for normalization of the theoretical backscattering amplitude function.[18] The EXAFS measurements of the reference material was performed at the same temperature immediately after the measurements for Can-Se.

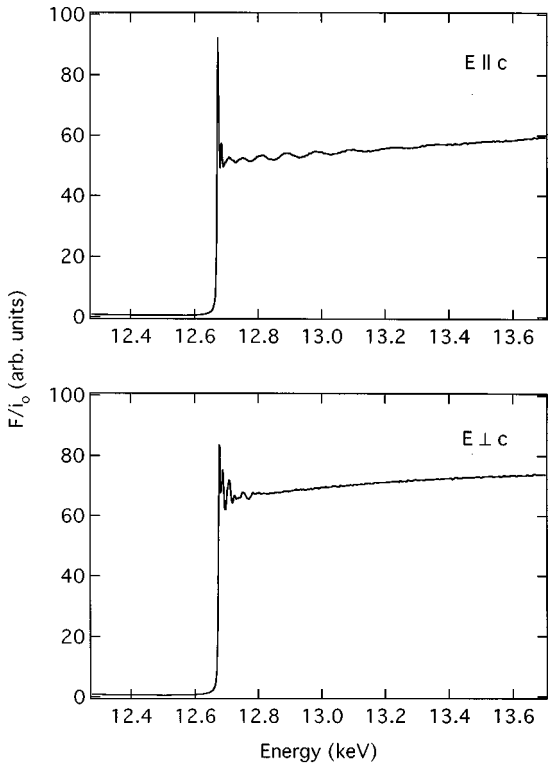

FIG. 1. Se *K*-edge fluorescence yield spectra for Can-Se ($E \| c$, top and $E \perp c$, bottom) taken using a 19-element solid-state detector array and a 27-pole wiggler at the Photon Factory.

III. RESULTS

Figure 1 shows the raw Se K_α fluorescence yield spectra taken at 30 K for Can-Se oriented with the electric vector of the x-ray beam parallel (top) and perpendicular (bottom), respectively, to the *c* axis. Strong anisotropy is obvious. Figure 2 shows the corresponding Se *K*-EXAFS oscillations for the two orientations (top) as well as a corresponding spectra for a powdered sample (bottom) after subtraction of smooth backgrounds due to the atomic absorption from the fluorescence yield spectra. The background function given as a combination of the third and forth order polynomials, with tabulated coefficients (Victoreen Function) which smoothly interpolate EXAFS oscillations using a cubic spline method, was normalized to the edge jump and subtracted from the fluorescence yield spectra. A strong anisotropy is obviously observed: In the *k* range from 5 to 16 $Å^{-1}$ the envelope functions of Can-Se ($\mathbf{E} \| c$) and *a*-Se agree very well in that both posses a maximum at $k = 5-6$ $Å^{-1}$.

In the spectra of Can-Se for the orthogonal orientation ($\mathbf{E} \perp c$), no oscillations are observed in the region, which is characteristic of selenium-selenium interaction. Instead, EXAFS oscillations are observed at much smaller *k* values, their amplitude decreasing rapidly. The present EXAFS oscillations are somewhat different from those for the same system previously reported in Ref. 11. Variation of the spline knots and inclusion of smaller *k* region for the $\mathbf{E} \perp c$ orientation has allowed us to improve the background subtraction, which is evidenced by disappearance of the peaks located at about 1 Å in the results of Fourier transform discussed below.

The spectrum for a powdered sample looks as an interme-

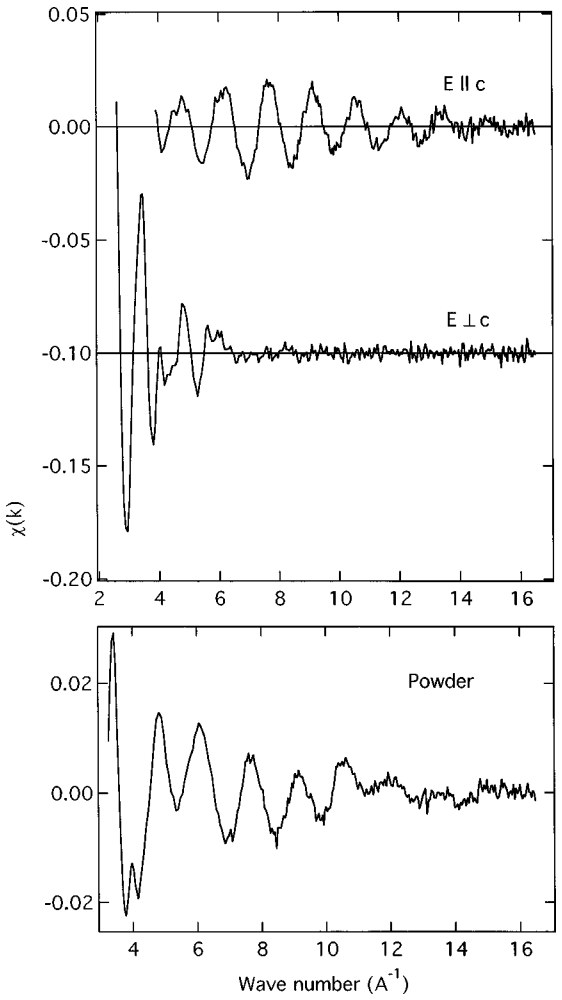

FIG. 2. Se *K*-edge EXAFS oscillations for single-crystal Can-Se (top) and powder (bottom) plotted as a function of photoelectron wave number *k*.

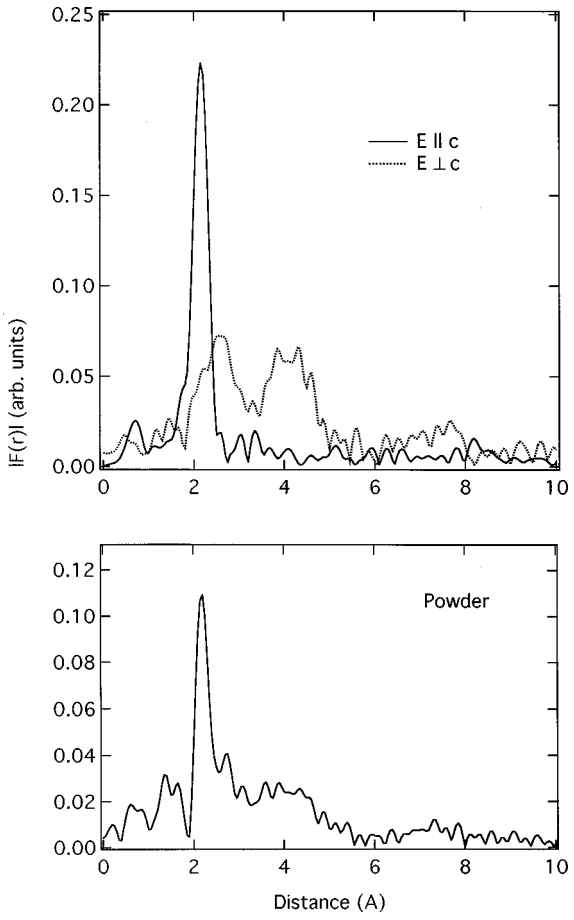

FIG. 3. Magnitude of Fourier transform of Se *K*-EXAFS oscillations multiplied by *k* for Can-Se. Top—single crystal. (Solid line and dotted line indicate the results for $\mathbf{E}\|c$ and $\mathbf{E}\perp c$, respectively.) Bottom—powder.

diate of the two spectra for a single crystal.

The EXAFS oscillations multiplied by k $[k\chi(k)]$ were Fourier transformed using the region extending from 4 to 16 Å^{-1} for $\mathbf{E}\|c$ and 3 to 16 Å for $\mathbf{E}\perp c$. The results for the single crystal and powder are shown in Fig. 3. One can see that for the sample orientation with channels parallel to the electric vector of the x-ray beam ($\mathbf{E}\|c$) there is one strongly pronounced peak representing the Se-Se interaction with no second or third peak observed. The other spectrum ($\mathbf{E}\perp c$) has several broad peaks at distances different from that of the Se-Se bond length. The *k* dependence of the EXAFS oscillations suggests that these peaks represent the interaction of Se atoms with the cancrinite channels and/or Na ions and OH groups contained in the channels. In the spectrum for the powder (bottom) which, again, is close to an average of the two spectra for the single crystal, both Se-Se interaction and interaction with the matrix are present.

EXAFS data analysis was performed by the a TSS-based data analysis package ADA (Ref. 19) written in FORTRAN-77 language with a graphical user interface using a mainframe computer. The least-squares curve fit was performed using the amplitude function calculated by FEFF6 (Ref. 20) and the empirical phase-shift function (polynomial). Coefficients of polynomial were determined so that the simulated data fit to the experimental one for the reference (a-Se) for which the Se-Se bond length was previously determined.[21] The errors in obtained values of the bond length, coordination number and mean-square relative displacement (MSRD) have been determined as follows. First, the statistical error was evaluated by the criterion that the error is given as the deviation of one parameter, which gives the twice larger residue. The systematic error was estimated from repeated measurements on the same sample. The estimated error limit was finally obtained by the convolution of the two contributions.

To analyze the data quantitatively, the Fourier-transformed data were filtered in order to extract the contribution of the first nearest neighbors, and back Fourier transformed into the *k* space. The filtered data for the first shell of Can-Se ($\mathbf{E}\|c$) together with the result of the least-squares curve fitting based on a single-scattering theory[22] are shown in Fig. 4. The curve fitting analysis gives the bond length of 2.40 ± 0.01 Å and the coordination number of 3.1 ± 0.6 for Can-Se, *assuming isotropic orientation of selenium chains*. The mean-square relative displacement (MSRD) for the Se-Se distance is comparable to that obtained for c-Se.[23] This indicates that the Se-Se bond has a short-range order comparable with a covalent single bond.

Figure 5 shows the average coordination number for the Se-Se interaction measured on a single crystal with different

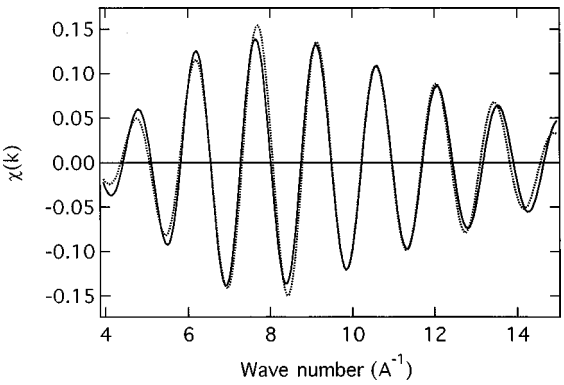

FIG. 4. Fourier-filtered first-shell Se K-EXAFS oscillations for Can-Se ($E\|c$) (solid line) and the result of the least-squares curve fitting (dashed line).

orientations of the sample. A decrease in the average Se-Se coordination with an increase in the angle between the c axis and E vector is clearly seen. One can expect the effective coordination number $3N\cos^2\theta$ to be three for a perfectly oriented dimer ($N=1$) when the E vector coincides with the orientation axis. This is a strong evidence that Se atoms form a linear array of *dimers* with negligible amount of other forms.

Similar data analysis performed on the crushed sample gives the bond length of 2.40 ± 0.01 Å (same as for the single crystal), average coordination number of 1.4 ± 0.3 and the MSRD similar to that of the single-crystal sample. A possible reason for a somewhat larger coordination number obtained for the crushed sample is discusses later.

In order to investigate the anisotropy we have also measured XANES spectra at different angles θ between the cancrinite c axis and the E vector of the x-ray beam. The obtained spectra (Fig. 4 of Ref. 11) exhibit two features. A near-edge peak (A) at 12 667 eV, corresponding to the white line of bulk selenium, decreases as θ increases and disappears completely for the sample oriented with the c axis perpendicular to the electric vector of the x-ray beam. This process proceeds in parallel with an appearance and growth of another peak (B) at 12 672 eV indicating that the two peaks are negatively correlated.

Figure 6 shows the result of deconvolution of the measured spectra for three different orientations, namely $\mathbf{E}\|c$ (top), $\mathbf{E}\perp c$ (bottom) and for the 45° angle between E and c (middle), into Lorentzian functions describing the transitions to bound states and the Fermi function corresponding to the continuum states. The deconvolution was performed so that the two Lorentzian peaks with variables (intensity, position, and width for each peak) were fit to the near-edge region, which is not affected by the EXAFS oscillations. It was found that the empirical continuum function shown in a dash-dot line in Fig. 6 gives a constant threshold value in energy, which justifies the procedure of deconvolution.

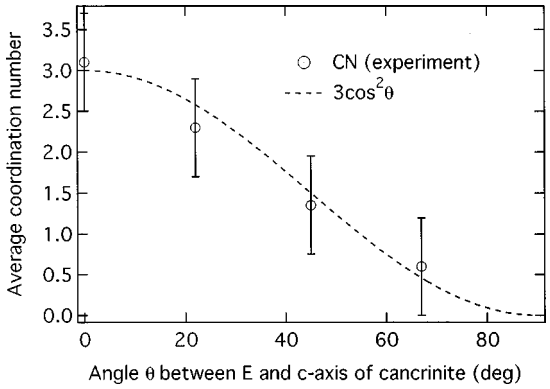

FIG. 5. Average Se-Se effective coordination number N^* as a function of the angle between E vector and cancrinite c axis calculated in the assumption of isotropic sample.

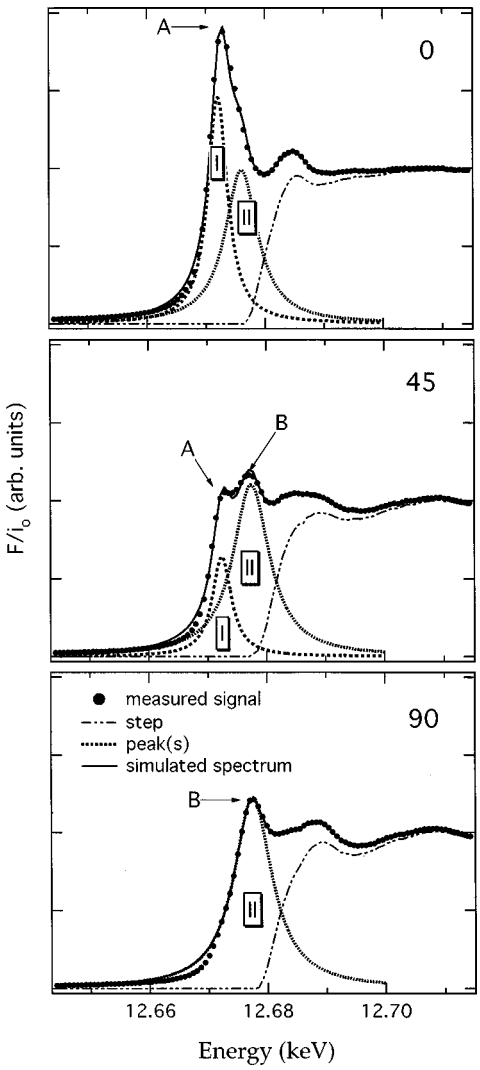

FIG. 6. Measured spectra (dots) and deconvolution into the boundlike states (dotted lines) and the steplike continuum state function (dashed-dotted line) for three different angles θ between the electrical field vector E and the c axis. The corresponding angles are marked in the top-right corner of each spectrum. The solid line indicates the fitted curve using the Lorentzian distributions (bound states) and the Fermi functions (continuum).

One can see that although the intensity of the peak related to feature A is strongly orientation dependent, the intensity of the peak fitting the feature B hardly varies indicating that the electron wave function corresponding to that peak has no preferred orientation. The steplike contribution of continuum states (in the shown energy range, which is much below the EXAFS region) is essentially identical in all cases. The full width at half maximum of the deconvoluted Lorenzian peak

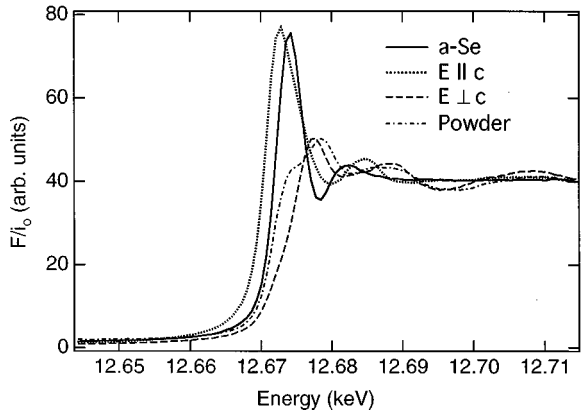

FIG. 7. Comparison of the XANES spectra for Can-Se and *a*-Se.

A is 4.1 eV in good agreement with the energy resolution discussed earlier.

In order to analyze the polarization dependence quantitatively we have applied simple formulas of Ref. 24 and we have found[11] that the best fit is obtained for $\alpha = 0°$ indicating that Se-Se bonds are highly oriented in the direction parallel to the *c* axis of the cancrinite.

In Fig. 7, the near-edge features for the Can-Se and *a*-Se are compared. One can find that the energy position for peak *A* for the single crystal Can-Se lies at lower energy than that of *a*-Se. In the data for the crushed Can-Se sample, the energy shift is not, however, clearly observed. Similar to EXAFS, the XANES spectrum for the powder sample looks intermediate between those for the single crystal. Figure 8 shows the measured XANES spectrum and that calculated from the single-crystal data assuming $\frac{1}{3}$ contribution from the ($\mathbf{E} \| c$) and $\frac{2}{3}$ from ($\mathbf{E} \perp c$) orientations. Taking into account the accuracy in the orientation of the single crystal ($\pm 5°$) and the fact that single crystal and powder are *different* samples (with somewhat different loading and background signal), the overall agreement is quite good.

We now turn our attention to the temperature dependence of EXAFS ($\mathbf{E} \| c$). This question is of special interest since the results of a Raman study[4–8] of Can-Se suggested the presence of structural transformations in the temperature

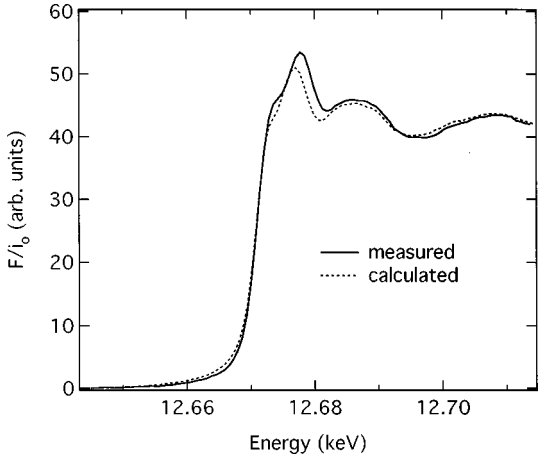

FIG. 8. XANES spectra for powdered Can-Se: measured (solid line) and calculated from those for the single crystal (dashed line).

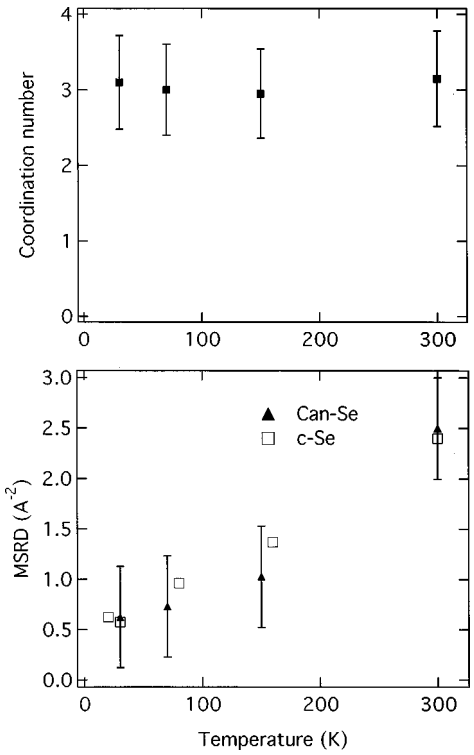

FIG. 9. Temperature dependence for the effective coordination number (top column) and MSRD (lower column) for the Se-Se correlation in Can-Se ($\mathbf{E} \| c$). For comparison, similar dependence (MSRD) for crystalline selenium (*c*-Se) is shown.

range between 20 and 300 K resulting from incommensurability between selenium chains and cancrinite. It was argued that a competition between intrachain dimer-dimer interaction and chain-matrix interaction occurs. According to this, some changes in dimer arrangement should take place and we can expect some effects in EXAFS corresponding to the second nearest-neighbor distance. However, we could not observe the second nearest-neighbor distance. We analyzed temperature dependencies of the coordination number and mean-square relative displacement (MSRD) corresponding to the first nearest neighbor. In Fig. 9, the effective coordination number N^* and MSRD are plotted as a function of temperature. Our results show that there is no noticeable change of coordination as the temperature is changed from 30 to 300 K: N^* remains *practically unchanged in the whole temperature range*, which indicates that the dimers are stabilized throughout this temperature range. The MSRD monotonically increases with the temperature increase as a result of increased amplitude of Se-Se intradimer vibrations.

IV. DISCUSSION

A. Polarized EXAFS

Remarkable anisotropy is obvious from comparison of spectra of the single-crystal Can-Se shown in Figs. 2 and 3. Comparison of the Se *K*-EXAFS for Can-Se ($\mathbf{E} \| c$) and *a*-Se (Ref. 23) shows that the envelopes of the two spectra are similar, which should be the case since the envelope is determined by the chemical nature of scatterers and selenium is the nearest scatterer in both cases. Quantitative analysis of the Fourier-transformed (and filtered) data gives the Se-Se

bond length of 2.40 ± 0.01 Å for Can-Se, while that for bulk Se equals 2.36 ± 0.01 Å for a crystal and 2.32 ± 0.01 Å for *a*-Se. Such an increase in the bond length is very unusual, since, in the case of confined selenium, interchain interaction is weakened and intrachain interaction is reinforced resulting in a decrease in the bond length, provided the chemical nature of bonding remains unchanged. Such a decrease in the bond length resulting from removal of interchain interaction was reported earlier for isolated Se chains confined in mordenite channels.[25] The observed increase in the bond length possibly implies a change in the chemical nature of bonding, such as appearance of strong interaction between selenium atoms and the cancrinite matrix.

Complete absence of Se-Se interactions for the other orientation ($\mathbf{E} \perp c$) suggests that Se forms *linear* structures. The obtained effective coordination number of 3.1 ± 0.6 for the ($\mathbf{E} \| c$) configuration using the isotropic reference sample becomes $\sim 1.0 \pm 0.2$ for the case of a linear arrangement of Se atoms, which means that each selenium atom has one neighbor, i.e., indeed, dimers are formed in the channels. This value for the coordination number agrees well with the number obtained for the crushed (isotropic) sample: 1.4 ± 0.3. Taking into account the fact that in the crushed sample we simultaneously determine the Se-Se and the Se-matrix interaction in other directions the two results are consistent.

In sharp contrast to the results previously reported for linear polyions in $(CH)_x$ (Ref. 27) the second nearest-neighbor Se-Se correlation is not observed in the spectrum for $\mathbf{E} \| c$ (Fig. 3, top). Strong focusing effect due to multiple scattering results in enhancement of interference for the second nearest neighbor in a linear chain[28] and the magnitude of the second nearest-neighbor peak is used to estimate the number of atoms in a chain. Its complete absence in our case independently suggests that selenium forms not continuous linear chain but strongly oriented dimers that are not equally spaced along the *c* axis. Alternative explanations could be either very large thermal motion of dimers or a large $(Se_2) \ldots (Se_2)$ distance. While the former can be possibly ruled out by the absence of any temperature dependence of EXAFS, the latter is quite possible.

In Fig. 3 ($\mathbf{E} \perp c$), one can observe two broad peaks centering at approximately 2.5 Å and 4 Å. These peaks correspond to the interactions between Se atoms and light element atoms forming the host matrix, i.e., Si, Al, and O atoms and ions such as OH groups and Na cations.

Recent studies[10] have revealed that Se and OH groups belong to different regions of the crystals. A possible range of Se-Na distance (3.00–3.26 Å) in the crystal structure determined from x-ray diffraction[10] matches the phase-shift corrected first-peak position in the Fourier transform (ca. 3 Å). It should be noted that the Se-Na distance in Na_2Se_2 (2.948 Å) is close to this value.

Three oxygen cites (O1, O3, O4) are located at around 4.4–4.5 Å in the radial distribution function calculated for the average structure, while there are other atoms (Si, Al) at slightly distant positions (4.8–5.0 Å). Because of insufficient resolution in *r* space due to the limited range in *k*, these two peaks are expected to appear as the double-peak structure separated by approximately 0.5 Å. The double-peak structure separated by 0.4 Å in the Fourier transform at around 4 Å is thus likely due to these correlations.

Summarizing the results of the Fourier transform for the perpendicular orientation, the overall agreement between the x-ray diffraction data[10] and EXAFS is reasonably good.

According to x-ray diffraction data,[10] the electron density of Se atoms displays three broad overlapping peaks. These peaks are interpreted as a result of distribution of Se dimers along the channel. It is difficult to determine precisely the bond length from the present x-ray diffraction data.[10] Further x-ray diffraction studies based on symmetry lower than $P6_3$ space group symmetry and with resolution better than it that of Ref. 10 are necessary.

We can thus conclude from the polarized EXAFS study that selenium forms dimers, which are perfectly oriented along the channel and the dimer-dimer distance is not unique indicating the incommensurate structure.

B. Polarized XANES

Analysis of the angular dependence of XANES spectra provides further evidence that selenium chains in cancrinite channels are strongly anisotropic. The best fit for the peak *A* angular dependence is obtained for $\alpha = 0°$, which means that Se-Se bonds are oriented along the channels and do not form helical structures, which is usual in all known allotropic forms of selenium containing chain structural elements. This strong anisotropy of selenium chains gives grounds to the calculated value of the coordination number to be ~ 1.0.

The fact that the peak *A* strongly polarized along the channel and the possible LUMO (lowest unoccupied molecular orbital) for Se is $4p\sigma^*$, it is likely that the peak *A* corresponds to $4p\sigma^*$. The peak *B*, which has very weak polarization dependence and is located at higher energy, is probably related to higher level orbitals, i.e., Rydberg states.

To discuss the electron state of selenium species, it seems reasonable to compare the energy positions of the near-edge structures for crushed Can-Se and *a*-Se. The two *K*-absorption edges basically coincide implying the same (neutral) state of confined selenium species. It should be bared in mind, however, that direct comparison of the edge energy positions may not be correct. Different from x-ray photoemission spectroscopy (XPS), where the energy between the core level and the vacuum level of an element in question is measured, in XANES, the measured value is the energy from the core level to the lowest unoccupied state (conduction band, or antibonding state). If the structure of the material is significantly changed or if the material is strongly anisotropic the energy position of the bottom of the conduction band also changes and selection rules for different polarizations may be different. One should thus compare transitions involving identical orbitals $[1s \Rightarrow 4p(\sigma^*)]$ and in our case the spectrum for *a*-Se has to be compared with transitions in the $\mathbf{E} \| c$ orientation of the Can-Se sample. This also clearly shows that isotropic samples for locally strongly anisotropic structures may lead to totally wrong conclusions regarding the charge state of the species.

Comparison of the edge positions for the Can-Se single crystal measured in $\mathbf{E} \| c$ orientation shows that the edge of the Can-Se is located at lower energies (by about 1.7 eV). Taking *a*-Se as a reference of charge on Se atom, this indicates that the electron density on Se atoms increases in the former sample, i.e., Se species are negatively charged. This

charging gives a most natural explanation as to why the bond length in Can-Se is larger than in bulk Se or in case of confinement of continuous (neutral) chains in nanochannels of mordenite. Previous result of an XPS study[10] has shown a decrease in the core-level binding energy by 1 eV for Can-Se. Taking this into account and assuming the same energy shift for different core levels our present data suggest that the final σ^* state in Can-Se is about 0.7 eV lower than that in bulk selenium. This result is consistant with the elongated Se-Se bond in Can-Se.

C. Mechanism of dimerization

Now, we turn our attention to the change in electron states caused by dimerization. As seen from Fig. 7, the lowest energy feature (peak *A*) observed in the XANES spectrum of Can-Se corresponds to the sharp bound-state-like peak in *a*-Se. In *a*-Se, two *p* orbitals are split into σ (bonding) and σ^* (antibonding) states, which lie below and above the nonbonding (lone-pair) orbitals, respectively. The lowest unoccupied states are σ^* for which the transition from 1*s* states is allowed within the dipole selection rule. Since excitations from Se 1*s* to σ^* are allowed by $E \| c$ but not by $E \perp c$, as the angle between the *c* axis and **E** increases, the intensity of peak *A* decreases. Theoretical calculation of XANES for two orthogonal orientations currently underway[29] give spectra that agree very well with the experimental ones.

We now consider possible models for the electron states associated with the dimerization. In the crystalline state, selenium forms helical chain structure with a dihedral angle of 100.6°. For an intercalated selenium chain in a nanochannel of cancrinite, however, interaction between the chain and a cage molecule forces the helical chain to be extended into a linear one (or prevents the formation of helical chains when Se dimers, which are majority species in the vapour phase, are incorporated into the cancrinite channels). Such a linear chain is unstable because of the repulsive interaction between lone pairs and bond charges. Removal of helicity would thus push up the energy levels of lone-pair electrons decreasing the energy of the antibonding states since *sp* mixing is not achieved because of lack in the overlap. In this case, one should expect a rearrangement of atoms such as bond breaking and dimerization, which would remove the instability in one of the following ways.

First, we consider a possibility of a double bond between the two selenium atoms. The corresponding molecular-orbital diagram for the Se_2 dimer, which is a triplet in the ground state,[30] is shown in Fig. 10(a). For Se_2 in the gaseous phase, a bond length (2.15 Å) has been found,[31] which is much shorter that the bond length observed in our case (2.40 Å). It is, thus, unlikely that the double bond formation takes place.

Another possibility is the formation of resonating charged defect states as illustrated in Fig. 10(b). In bulk selenium neutral dangling bonds are unstable and charged defects are formed due to negative correlation energy.[32,33] In the initial selenium dimers, two one-fold defect sites (C_1^0) are bonded together as nearest neighbors. It is, thus, plausible that neutral defects with dangling bonds can be stabilized by a dynamic charge transfer or resonating between the charged defect sites (C_1^+-C_1^-).

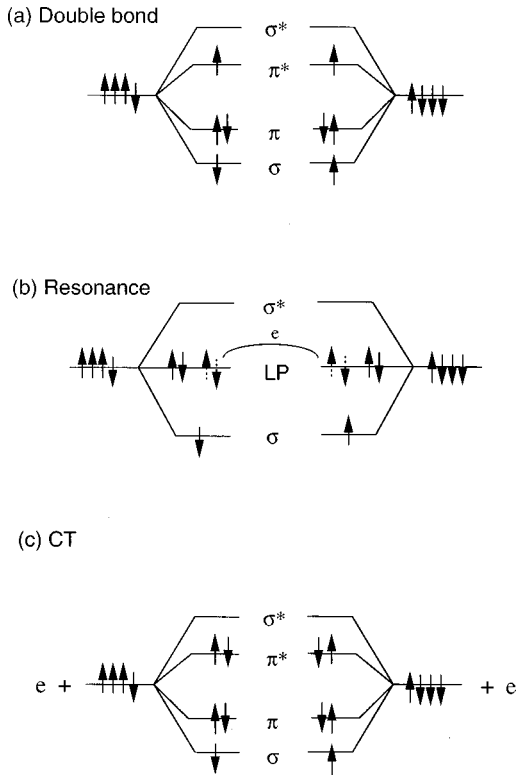

FIG. 10. Schematic MO diagram of selenium dimers in cancrinite. Unstable strained linear chains form dimers. Unpaired electrons can form a molecule with a double bond (a). Resonating between positively and negatively charged defects stabilizes the dimer structure (b). A charge transfer results in the closed-shell configuration of selenium atoms in Se_2^{-2} (c).

Finally, we consider a possibility of a chemical reaction between selenium and cancrinite such as the formation of chemical bonds and charge transfer [Fig. 10(c)]. Since the dimerization introduces one dangling bond to each selenium atom, hydroxyl group might terminate these bonds if they make covalent bonds. However, we have found no contribution from the interaction between Se atoms and light element atoms around the crystallographic distance between the Se atom and OH group (1.5 Å). This indicates that OH sites near Se dimers are not occupied. Further, the recent IR measurements on Can-Se (Ref. 10) demonstrated that OH groups are absent in samples heavily loaded with selenium.

The last and quite likely mechanism of stabilization is a charge transfer from Na species of the cancrinite matrix to Se atoms. The distance between Se atoms and the nearest-neighbor light element atoms is observed at about 3.0 Å, which is likely to be due to Na species for which the crystallographic Se-Na distance is 3.0–3.3 Å depending on the Se-atom position in the channel. In addition the obtained Se-Se distance is very close to that in a Na_2Se_2 crystal (2.38 ± 0.05 Å).[34] The absence of features at lower energies that could be ascribed to π^* states in XANES spectra is consistant with the MO diagram for the charge transfer. The decrease of OH concentration in Can-Se agrees with this mechanism, which achieves the charge neutrality. This possibility is also consistent with the conclusion of a recent x-ray photoemission spectroscopy (XPS) study, which suggested a presence of doubly charged dimers Se_2^{2-}.[4,10] In a recent paper[35] where selenium was introduced into cancrinite

during the synthesis, the authors also concluded that Se_2^{2-} species were present. Thus, we conclude that the charge transfer is quite likely to be the case.

The observed increase in Se-Se distance in oriented Se dimers in cancrinite by 0.25 Å compared to that in Se_2 in gaseous phase (2.15 Å) agrees well with the double negative charge on the dimer. It was reported that a negative charge transfer to a O_2 molecule increases the bond length $R_{O\text{-}O}$. $R_{O\text{-}O}$'s for O_2, O_2^-, and O_2^{2-} equal 1.21, 1.28, and 1.48 Å, respectively.[26] The removal of an electron, on the other hand, reduces the bond length and $R_{O\text{-}O}$ for O_2^+ is 1.12 Å resulting in the shortest one of all. This result indicates that in a simple dimer molecules such as O_2, the electron removal from an antibonding orbital strengthens the bond (increases the bond order) while the addition of an electron weakens it in agreement with the present observation that for negatively charged dimers, the bond length increases. The bond length difference between Se_2^{2-} and Se_2 (11.5%) is much smaller than that for oxygen (22%) reflecting the spatial extention of bond orbitals.

V. CONCLUSIONS

Our x-ray absorption study of selenium chains confined in cancrinite enabled us to make the following conclusions regarding the structure of selenium confined in nanochannels of cancrinite. (1) Strong polarization dependence for Can-Se single crystals provides direct experimental evidence for linear orientation of Se-Se bonds along the channel of cancrinite. This kind of information is not obtainable if one measures the EXAFS for a powder. This result also demonstrates that previous EXAFS experiments on Se confined in different zeolite powders have to be reconsidered as to completeness and reliability of the information they provide. (2) Selenium confined in nanochannels of cancrinite forms weakly interacting linearly arranged dimers and not continuous chains. (3) The obtained Se-Se bond length (2.40 Å) for Can-Se is larger than in any other known form of selenium. (4) Polarized XANES clearly demonstrates that Se dimers are oriented parallel to the channel of cancrinite. Fitting of the XANES spectra indicates the existance of two types of boundlike states: one being strongly polarized along the *c* axis and the other one being essentially isotropic. Comparison of XANES for Can-Se with that for bulk selenium indicates a negative charge transfer to Se dimers (most likely from Na species) which also explains an increased Se-Se bond length in Can-Se. Comparison of spectra for single crystal and powder clearly shows that isotropic samples for locally strongly anisotropic structures may lead to totally wrong conclusions regarding the charge state of the species. (5) Despite a strong temperature dependence of Raman scattering, which suggested several phase transitions, no change was detected in EXAFS showing that the basic structure of dimers is unchanged within the whole temperature range.

ACKNOWLEDGMENTS

This work, partly supported by NEDO, was performed in the Joint Research Center for Atom Technology (JRCAT) under the joint research agreement between the National Institute for Advanced Interdisciplinary Research (NAIR) and the Angstrom Technology Partnership (ATP). The measurements were done at the Photon Factory as part of the research project No. 95G026. The authors are grateful to Professor V.N. Bogomolov (Ioffe Institute) for provision of (hydro)cancrinite single crystals used in this study. A very useful discussion on the correlation between the charge state and energy position of the *K*-absorption edge with Professor A. Bianconi (University of Rome) is gratefully acknowledged. The authors also wish to thank Dr. Y. Shimoi (ETL) for useful discussions.

*On leave from A. F. Ioffe Physico-Technical Institute, St. Petersburg, Russia.

[1] V. N. Bogomolov, Usp. Fiz. Nauk **124**, 171 (1978) [Sov. Phys. Usp. **21**, 77 (1978)].

[2] G. D. Stucky and J. E. MacDougall, Science **247**, 669 (1990).

[3] G. A. Ozin, Adv. Mater. **4**, 612 (1992).

[4] V. V. Poborchii, in *Progress in Zeolite and Microporous Materials Studies in Surface Science and Catalysis*, edited by H. Chon, S. K. Ihm, and Y. S. Uh (Elsevier Science, Amsterdam, 1997), Vol. 105, p. 631.

[5] V. V. Poborchii, *Proceedings of the 1st Japan-USSR Meeting Material Design Using Zeolite Space, Kiryu, Japan, 1991*, edited by M. Sato (Gunma University, Kiryu, 1991), p. 1.

[6] V. N. Bogomolov, A. N. Efimov, M. S. Ivanova, V. V. Poborchii, S. G. Romanov, Yu. I. Smolin, and Yu. F. Shepelev, Fiz. Tverd. Tela (Leningrad) **34**, 1722 (1992) [Sov. Phys. Solid State **34**, 916 (1992)].

[7] V. V. Poborchii, J. Phys. Chem. Solids **55**, 737 (1994).

[8] V. V. Poborchii, M. S. Ivanova, and S. S. Ruvimov, in *Proceedings of the 10th International Zeolite Conference, Garmischpartenkirchen, Germany, 1994*, edited by J. Weitkamp, H. G. Karge, H. Pfeifer, and W. Hölderich (Elsevier, Amsterdam, 1994), Vol. 84, p. 2285.

[9] Yu. A. Barnakov, A. A. Voronina, A. N. Efimov, V. V. Poborchii, and M. Sato, Inorg. Chem. **31**, 748 (1995).

[10] V. V. Poborchii, M. Sato, and A. V. Shchukarev, Solid State Commun. **103**, 649 (1997).

[11] A. V. Kolobov, H. Oyanagi, V. V. Poborchii, and K. Tanaka, Solid State Commun. **103**, 669 (1997).

[12] H. Oyanagi, K. Haga, and Y. Kuwahara, Rev. Sci. Instrum. **67**, 350 (1996).

[13] T. Oversluizen, T. Matsushita, T. Ishikawa, P. M. Stefan, S. Sharma, and A. Mikuni, Rev. Sci. Instrum. **60**, 1486 (1989).

[14] H. Oyanagi, Y. Kuwahara, and H. Yamaguchi, Rev. Sci. Instrum. **66**, 4482 (1995).

[15] S. Sasaki, S. Yamamoto, T. Shioya, and H. Kitamura, Rev. Sci. Instrum. **60**, 1859 (1989).

[16] H. Oyanagi, M. Martini, and M. Saito, Nucl. Instrum. Methods Phys. Res. A **403**, 58 (1998).

[17] H. Oyanagi, T. Matsushita, H. Tanoue, T. Ishiguro, and K. Kohra, Jpn. J. Appl. Phys., Part 1 **24**, 610 (1985).

[18] J. J. Rehr and E. A. Stern, Phys. Rev. B **14**, 4413 (1976); B. K. Teo, J. Am. Chem. Soc. **103**, 3990 (1981).

[19] H. Oyanagi (unpublished).

[20] J. J. Rehr, S. I. Zabrinsky, and R. C. Albers, Phys. Rev. Lett. **69**, 3397 (1992).

[21] A. Kolobov, H. Oyanagi, K. Tanaka, and Ke. Tanaka, Phys. Rev. B **55**, 726 (1997).

[22] E. A. Stern, Phys. Rev. B **10**, 3027 (1974).
[23] A. V. Kolobov, H. Oyanagi, K. Tanaka, and Ke Tanaka, Phys. Rev. B **55**, 726 (1997).
[24] J. Stohr and R. Jaeger, Phys. Rev. B **26**, 4111 (1982).
[25] K. Tamura, S. Hosokawa, H. Endo, S. Yamasaki, and H. Oyanagi, J. Phys. Soc. Jpn. **55**, 528 (1986).
[26] S. C. Abrahams, Q. Rev., Chem. Soc. **10**, 407 (1956).
[27] H. Oyanagi, M. Tokumoto, T. Ishiguro, H. Shirakawa, H. Nemoto, T. Matsushita, M. Ito, and H. Kuroda, J. Phys. Soc. Jpn. **53**, 4044 (1984).
[28] N. Alberding and E. D. Crozier, Phys. Rev. B **27**, 3374 (1983).
[29] A. V. Soldatov and G. Yalovega (unpublished).
[30] C. Heinemann, W. Koch, G.-G. Linder, D. Reinen, and P. O. Windmark, Phys. Rev. A **54**, 1979 (1996).
[31] *American Institute of Physics Handbook* (McGraw-Hill, New York, 1982), pp. 7–181.
[32] S. G. Bishop, U. Strom, and P. C. Taylor, Phys. Rev. Lett. **36**, 543 (1975).
[33] A. V. Kolobov, M. Kondo, H. Oyanagi, R. Durny, A. Matsuda, and K. Tanaka, Phys. Rev. B **56**, R485 (1997).
[34] H. Von Foppl, E. Busmann, and F. K. Frorath, Z. Anorg. Allg. Chem. **314**, 13 (1962).
[35] G. G. Lindner, K. Hoffmann, K. Witke, D. Reinen, C. Heinemann, and W. Koch, J. Solid State Chem. **126**, 50 (1996).